Small-World Network Models of Intercellular Coupling Predict Enhanced Synchronization in the Suprachiasmatic Nucleus

Christina Vasalou, Erik D. Herzog and Michael A. Henson

J Biol Rhythms 2009; 24; 243
DOI: 10.1177/0748730409333220

Small-World Network Models of Intercellular Coupling Predict Enhanced Synchronization in the Suprachiasmatic Nucleus

Christina Vasalou,[*] Erik D. Herzog,[†] and Michael A. Henson[*]

[*]*Department of Chemical Engineering, University of Massachusetts, Amherst, Massachusetts,*
[†]*Department of Biology, Washington University, St. Louis, Missouri*

Abstract The suprachiasmatic nucleus (SCN) of the hypothalamus is a multioscillator system that drives daily rhythms in mammalian behavior and physiology. Based on recent data implicating vasoactive intestinal polypeptide (VIP) as the key intercellular synchronizing agent, we developed a multicellular SCN model to investigate the effects of cellular heterogeneity and intercellular connectivity on circadian behavior. A 2-dimensional grid was populated with 400 model cells that were heterogeneous with respect to their uncoupled rhythmic behavior (intrinsic and damped pacemakers with a range of oscillation periods) and VIP release characteristics (VIP producers and nonproducers). We constructed small-world network architectures in which local connections between VIP producing cells and their 4 nearest neighbors were augmented with random connections, resulting in long-range coupling across the grid. With only 10% of the total possible connections, the small-world network model was able to produce similar phase synchronization indices as a mean-field model with VIP producing cells connected to all other cells. Partial removal of random connections decreased the synchrony among neurons, the amplitude of VIP and cAMP response element binding protein oscillations, the mean period of intrinsic periods across the population, and the percentage of oscillating cells. These results indicate that small-world connectivity provides the optimal compromise between the number of connections and control of circadian amplitude and synchrony. This model predicts that small decreases in long-range VIP connections in the SCN could have dramatic effects on period and amplitude of daily rhythms, features commonly described with aging.

Key words SCN, circadian, graph theory, small world, intercellular communication, synchronization, senescence

The suprachiasmatic nucleus (SCN) of the hypothalamus is the mammalian circadian pacemaker responsible for the temporal organization of a number of physiological and behavioral rhythms. Circadian rhythmicity is ensured not only by autonomous intracellular mechanisms within individual cells (Reppert and Weaver, 2002) but also by intercellular communication that coordinates functionally and structurally distinct cell types across the SCN (Low-Zeddies and Takahashi, 2001). Vasoactive intestinal polypeptide (VIP) is a critical neuropeptide responsible for the generation of circadian rhythms and the synchronization of

1. To whom all correspondence should be addressed: Michael A. Henson, Department of Chemical Engineering, University of Massachusetts, 686 North Pleasant Street, Amherst, MA 01003; e-mail: henson@ecs.umass.edu.

JOURNAL OF BIOLOGICAL RHYTHMS, Vol. 24 No. 3, June 2009 243-254
DOI:10.1177/0748730409333220

individual oscillations (Aton et al., 2005). VIPergic cells appear to make connections with other VIPergic neurons (Daikoku et al., 1992) as well as with neurons within the dorsomedial SCN (called the "shell") that express the neurotransmitter arginine vasopressin (AVP; Kalamatianos et al., 2004). AVP is abundantly synthesized within the shell, a region characterized by restricted dendritic arbors that are mostly confined between proximal neurons (Pennartz et al., 1998). By contrast, the ventrolateral SCN (called the "core") is characterized by a dense neural network with projections to distal areas across the SCN (Abrahamson and Moore, 2001). VIPergic projections originating from the densely innervated core and terminating within the sparsely and locally connected shell are therefore postulated to have a role in the coordination of the circadian signal across the SCN (Abrahamson and Moore, 2001).

The complexity of the SCN network arises not only from its large size but also from the complex dynamic behavior of each neuron and the heterogeneous connection topology linking individual oscillators. In an effort to trace the dynamics of such complex networks to their structural characteristics, techniques have been developed within the field of theoretical biology to allow the general mathematical representation of numerous biological and natural networks (Albert and Barabasi, 2002; Strogatz, 2001). Various neural systems in the brain have been shown to be adequately characterized by "small-world" networks (Netoff et al., 2004). The small-world topology combines local circuits of tightly coupled cells with random connections between cells, thereby introducing long-range connections that substantially reduce the average path length between cells (Newman et al., 2000; Watts and Strogatz, 1998).

One of the most important attributes of the small-world topology is its ability to express robust and synchronous signals as readily as fully connected networks. Small-world networks, however, contain a much lower degree of interconnectedness when compared with the mean-field model and are therefore considered as low "energy budget" organizations. Wiring distant neurons across the brain is a costly mechanism, which depends on many parameters, such as the network volume (Cherniak, 1992; Mitchison, 1991) or the metabolic requirements (Attwell and Laughlin, 2001). Signal transmission via action potentials requires high energy expenditure and therefore neural networks are assumed to evolve and organize their structures following the principle of wiring economy (Attwell and Laughlin, 2001).

Several mathematical models have been developed to characterize the coupled dynamics underlying the mammalian circadian clock (Bernard et al., 2007; Gonze et al., 2005; Antle et al., 2003). These multicellular computational models typically consist of mathematical descriptions of circadian gene expression and intercellular coupling. The various models differ in their choice of single cell oscillator models, utilizing either simple limit-cycle oscillators such as the Van der Pol model (Antle et al., 2003), or detailed descriptions of transcriptional and translational feedback loops (To et al., 2007; Bernard et al., 2007). Other points of distinction are the coupling intercellular mechanism and the topology of the simulated network. Representative studies include locally coupled (Kunz and Achermann, 2003; Bernard et al., 2007; To et al., 2007), mean-field (Gonze et al., 2005), and random network (Bernard et al., 2007) architectures. To our knowledge, this article represents the 1st study on the incorporation of a detailed single cell oscillator model into a heterogeneous network of coupled oscillators to investigate how network topology affects system behavior and circadian dynamics.

In an effort to discover the interplay between connectivity and behavioral or physiological attributes of the circadian system, the present study has been devoted to regenerating and mimicking the spatiotemporal organization of the SCN. Topological features of the neural network are assumed to affect the transmission and synchronization of circadian signals across the SCN. Our focus has been on constructing a broad range of connectivity patterns and attempting a correlation between various network architectures and observed behavioral phenotypes. For the purpose of this study a previously developed multicellular model (To et al., 2007), comprised of a detailed molecular description of a single circadian neuron and a VIP-instigated signaling cascade, was utilized. Network architectures, ranging from the nearest neighbor scheme to the mean-field model, were characterized via their connection density, defined as the average number of links per neuron, and their extent of long-range wiring, which was reflected by the normalized length of all links connecting non-neighboring cells across the population. Our main objective was to quantitatively evaluate the importance of such connectivity patterns, to correlate connectivity with behavioral outputs, and to investigate small-world networks as an "optimal" topology capable of producing coherent signaling with a small wiring cost compared with globally connected networks.

Our study was limited to VIP signaling because of its demonstrated importance in synchronizing SCN neurons and anatomical evidence suggesting the presence of both short-range and long-range VIP-mediated connections in the SCN. Although we acknowledge that other signaling mechanisms are likely involved in rhythm generation, we believe that the conclusions reached for VIP signaling would be applicable to other signaling mechanisms that include both short-range and long-range connections.

MATERIALS AND METHODS

Intracellular Oscillator Model

The core oscillator utilized in our model originates from a previous study (Leloup and Goldbeter, 2003) and consists of 16 ordinary differential equations in time that describe intertwined negative and positive regulatory transcriptional loops involving the key genes of the circadian clock. Transcription of the *Per* and *Cry* genes is activated by a heterodimer formed from the CLOCK and BMAL1 proteins. This activation is rhythmically suppressed and reestablished by a complex of the PER and CRY proteins, which blocks the activity of CLOCK/BMAL1 dimers and negatively autoregulates transcription of the *Per* and *Cry* genes. Our model did not include the loop involving *Reverbα* inasmuch as it is not required for sustained circadian oscillations.

Treatments that desynchronize the rhythms among SCN neurons have revealed that approximately 30% of the population behaves as pacemakers and that these neurons produce a wide range of intrinsic periods (Aton et al., 2005). In an effort to produce cellular heterogeneities consistent with such experimental findings, we altered core oscillator parameters used in the original reference (Leloup and Goldbeter, 2003). Random perturbations in the basal *Per* transcription rate (ν_{sp0}) were introduced to create an uncoupled population in which about 40% of the model neurons were intrinsic oscillators. Based on results from a sensitivity analysis conducted with the core oscillator model, the *Bmal1* transcription rate (ν_{sB}), and the *Bmal1* mRNA degradation rate (ν_{mB}) were determined to have the largest effect on the single cell oscillation period (S. Taylor, personal communication, September 2007). Therefore, the ν_{sB} and ν_{mB} parameters were randomly perturbed to achieve a distribution of periods among the intrinsic oscillators with their uncoupled periods ranging between 18 and 30 h as observed experimentally (Aton et al., 2005).

Intercellular Coupling Model

We utilized a revised VIP signaling cascade model from our previous study (To et al., 2007) to establish intercellular coupling between the model neurons. Because VIP is known to be rhythmically released (Dardente et al., 2004), the VIP release rate was assumed to have a constant phase relationship to the *Per* mRNA concentration (To et al., 2007). In our previous study (To et al., 2007), we assumed that released VIP affected other cells through a diffusional process such that VIP released from a given cell had a greater effect on adjacent cells than cells located further away. Because released VIP is actually transmitted to other cells via synaptic connections, we modified the signaling model such that the VIP concentration sensed by each neuron and available to bind its VPAC2 receptors was computed as

$$\gamma_i(t) = \frac{1}{k_i} \sum_{j=1}^{N} a_{ij} \rho_j(t) \qquad (1)$$

where γ_i is the VIP concentration sensed by neuron i, k_i is the number of synaptic inputs received by neuron i, N is the total number of neurons in the population, and α_{ij} is a binary coupling term that assumed a value of 1 when a connection between neuron j and i was present and was zero otherwise. VIP binding to the VPAC2 receptor was assumed to form a complex that initiated a signaling cascade, which involved a number of steps ultimately producing activation of *Per* transcription. Photic input was assumed to activate calcium and enhance *Per* transcription through the same cascade. Additional details about the signaling model are contained in our original study (To et al., 2007). The effective coupling strength between connected neurons was determined by parameters of the VIP signaling cascade and was not varied between simulations to allow focus on architecture effects.

Cellular Network Model

Small-world networks were constructed through the following procedure, which extends an established method for 1-dimensional lattices (Newman, 2000) to the 2-dimensional grids used in this study. An ensemble of heterogeneous cells was placed on an equally spaced 2-dimensional grid to mimic the spatial organization of the SCN. Each neuron was connected to its 4 nearest neighbors to establish local connections (Fig. 1A). End effects on the grid were eliminated by

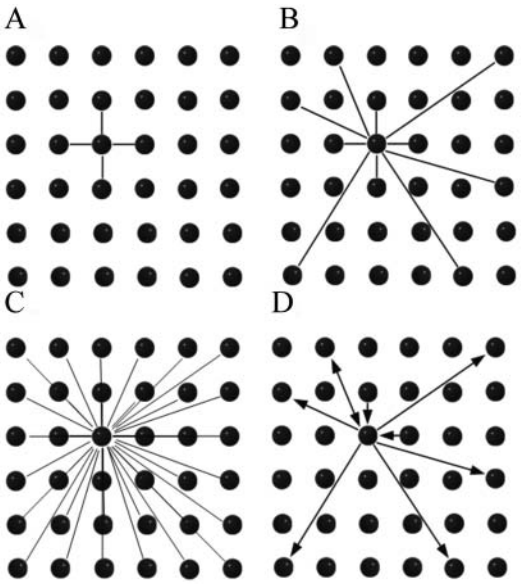

Figure 1. A schematic representation of the procedure used to construct different cellular networks on a 2-dimensional grid. (A) A nearest neighbor network with each neuron connected to its 4 nearest neighbors and vasoactive intestinal polypeptide (VIP) expressed by all cells within the network. (B) Small-world network with additional shortcut connections added to the nearest neighbor network according to a probability *p* and VIP expressed by all cells within the network. (C) Mean-field network with each neuron connected to every other neuron and VIP expressed by all cells within the network. (D) The small-world network that results when VIP production is randomly eliminated from a fixed percentage of neurons, yielding a heterogeneous network with both reciprocal and nonreciprocal connections.

implementing periodic boundary conditions such that neurons located at an edge were connected to corresponding neurons at the opposite side of the grid, producing a symmetrical lattice where all neurons regardless of their location contained 4 connections. Additional connections (known as shortcut connections) were established at the beginning of each simulation between random pairs of cells according to a probability *p*. We did not consider changing topologies during individual simulations because such network adaptation would be very slow compared with the circadian time scale.

The extreme values of p produced the nearest neighbor topology ($p = 0$; Fig. 1A) and the mean-field topology ($p = 1$), a fully connected grid where every neuron was coupled to every other neuron (Fig. 1C). Intermediate probability values produced networks between these 2 extremes, with values in the range $0.01 < p < 0.1$ referred to as small-world network topologies (Newman, 2000; Fig. 1B). Following graph theory (Sporns et al., 2004), we did not allow multiple connections between the same neuron pairs (α_{ij} could not be greater than 1) or connections of a neuron with itself (α_{ii} was always 0). The class of small-world networks considered in this study that are constructed through the addition of shortcut connections should not be confused with those involving random rewiring of existing connections (Watts and Strogatz, 1998). Although both types of graphs are commonly referred to as small-world networks, the addition of shortcuts offers the advantage that the network is ensured to remain completely connected whereas rewiring of connections can produce regions with no connections to the remainder of the network (Newman, 2000).

Networks developed through the procedure described above required the expression of VIP by all neurons across the grid and yielded connectivity patterns with reciprocal, undirected connections. However, VIP is known to be synthesized by approximately 20% of all SCN neurons (Moore et al., 2002) that make both reciprocal and nonreciprocal connections with other SCN neurons (Romijn et al., 1997). This source of heterogeneity was captured by randomly zeroing VIP production from 80% of the model neurons and eliminating all connections from these non-VIP-producing cells. Therefore, the 20% of VIPergic neurons could establish bidirectional connections, whereas the 80% of non-VIPergic neurons could only receive connections from other cells. These non-VIPergic, locally connected model neurons can be interpreted as AVPergic cells in the shell with restricted dendritic arbors that are mostly confined between neighboring neurons (Pennartz et al., 1998). The resulting directed graphs had nonreciprocal as well as reciprocal connections (Fig. 1D). Neurons on these directed graphs were coupled by making the binary coupling term α_{ij} (Eq. 1) unity when a connection between neuron j and i was present and zero otherwise.

We developed a measure to allow direct comparison of the prevalence of shortcut connections in the various networks considered in this study. The extent of long-range connectivity λ was computed as

$$\lambda = \frac{\sum_{i=1}^{N} \sum_{j=1}^{N} \nu_{ij}}{N} \qquad (2)$$

where ν_{ij} is the Euclidean distance between neurons i and j and N is the total number of neurons on the grid. Connections between the 8 nearest neighbors were regarded as short range and not included in the calculation of λ. The distance between vertically and horizontally adjacent cells was assigned 1 unit, and the

distance between diagonally adjacent cells was assigned $\sqrt{2}$ units. The Euclidean distance ν_{ij} was calculated by adding these incremental distances along the shortest path connecting the 2 cells with ν_{ii} assigned a value of zero. A normalized λ value was obtained by scaling the unnormalized value in Eq. 2 with the λ value calculated for the mean-field model, such that the normalized value ranged between 0 for the nearest neighbor model ($p = 0$) and 1 for the mean-field model ($p = 1$).

Computational Studies and Data Analysis

Dynamic simulations were performed by placing 400 cells on a 20 × 20 grid, resulting in a multicellular model with 6800 differential equations and 2000 algebraic equations. Nominal model parameter values were mostly obtained from the original references (To et al., 2007) on which our model was based. The signaling parameters a, representing the maximum VIP release, and K_D, representing the equilibrium dissociation constant, were changed from their original values of 10 nM and 2.5 nM (To et al., 2007) to 12 nM and 2 nM, respectively, in order to achieve maximum synchronization. The core oscillator parameter k_1 that determines the transport rate of the PER/CRY complex from the cytosol to the nucleus was changed from its original value of 0.4 nM (Leloup and Goldbeter, 2003) to 0.7 nM to obtain a single cell oscillation period of 24 h. Random perturbations in the basal *Per* transcription rate (ν_{sp0}) with 10% standard deviation around its nominal value were introduced to create an uncoupled population in which about 40% of the model neurons were intrinsic oscillators. The *Bmal1* transcription rate (ν_{sB}) and the *Bmal1* mRNA degradation rate (ν_{mB}) were randomly perturbed with a 2% standard deviation around their nominal values to achieve a distribution of periods among the intrinsic oscillators with their uncoupled periods ranging between 18 and 30 h as observed experimentally (Aton et al., 2005). Different network architectures were constructed by varying the probability for shortcut connections (p). Asynchronous initial cell states were generated using a previously published method for yeast cell populations (Henson, 2004).

The resulting multicellular model was formulated within MATLAB and solved using the differential-algebraic equation solver ode23. Simulations were allowed to run for 200 h (≥8 oscillation cycles) to provide sufficient results to assess synchronicity. For each p value, we constructed 10 network realizations for statistical calculation of structural and dynamic network properties. Two measures were used to assess the degree of synchronicity obtained from the various network models. The synchronization index (SI; Strogatz, 2000) quantifies the ability of the system to produce a coherent signal by comparing the instantaneous phase angle of each oscillator relative to a reference cycle, and the order parameter (R; Garcia-Ojalvo et al., 2004) represents the overall degree of synchrony over a specified time period. Both SI and R were computed from the *Per* mRNA concentrations of the core oscillator models. All R values were computed over a time period of 200 h (≥8 days).

RESULTS

Structural Properties of Small-World Networks

We varied the probability p of adding shortcut connections to determine the structural properties of the resulting cellular networks. Because VIP production was randomly eliminated in 80% of the neurons, each realization of the nearest neighbor model ($p = 0$) produced averages of exactly 1 incoming connection per neuron and 4 outgoing connections per VIPergic neuron. The mean-field model ($p = 1$) contained much greater coupling with approximately 80 incoming connections per neuron and 400 outgoing connections per VIPergic neuron across 10 realizations. The average numbers of incoming and outgoing connections increased rapidly in the small-world region ($0.01 < p < 0.1$). Many of our subsequent analyses are based on the value $p = 0.05$, where 10 realizations produced an average of 8 incoming connections per neuron and 40 outgoing connections per VIPergic neuron or approximately 10 times less connections than in the mean-field model.

The extent of long-range connectivity λ (Eq. 2) was calculated for different p values to provide a quantitative measure of increased network coupling achieved through the addition of new connections to the nearest neighbor topology. Due to the normalization used, λ was identically 1 for $p = 1$ and much less than 0.01 for $p < 10^{-3}$. For our nominal value $p = 0.05$, 10 realizations of the small-world network produced an average $\lambda = 0.1$ with small standard deviation. This result was consistent with the observation that $p = 0.05$ yields approximately 10 times fewer connections than the mean-field model ($p = 1$).

Synchronization Behavior of Small-World Networks

We varied the probability p to determine the effect of adding shortcut connections on the synchronization

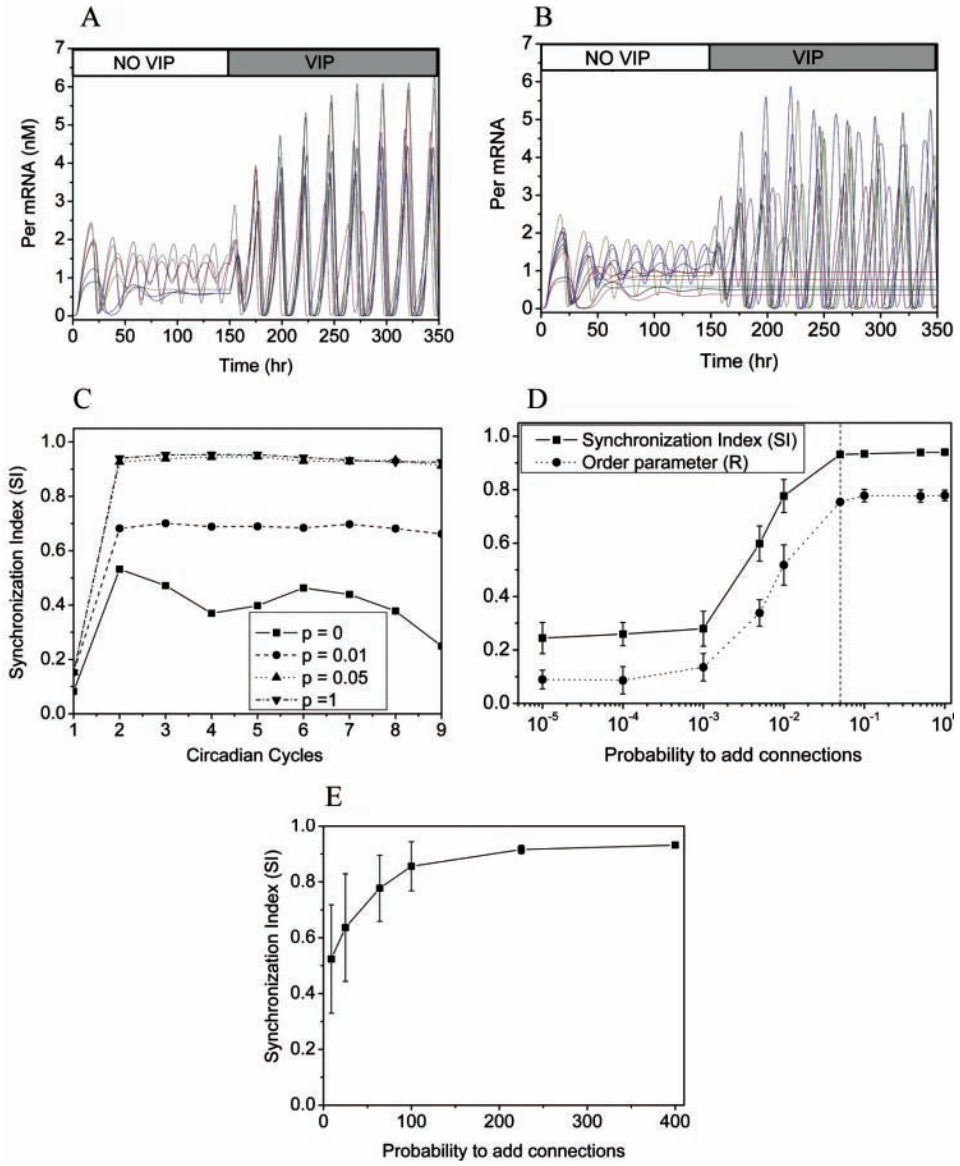

Figure 2. Synchronization behavior of cellular networks on a 2-dimensional grid when vasoactive intestinal polypeptide (VIP) is introduced at t = 150 h. (A) *Per* **mRNA time profiles of 10 randomly selected cells for the small-world network model (p = 0.05). All cells are rhythmic and the population exhibits a high degree of phase synchrony. (B)** *Per* **mRNA time profiles of 10 randomly selected cells with the nearest neighbor model (p = 0). Some cells are arrhythmic and the population exhibits a low degree of phase synchrony. (C) Synchronization index (SI) versus time for 4 values of the probability p, where circadian cycle 1 represents the time of VIP introduction. Despite having only 10% of the long-range connections, the small-world network model (p = 0.05) synchronizes as rapidly and achieves nearly the same final SI value as the mean-field model (p = 1). A small-world network model with fewer long-range connections (p = 0.01) yields lower SI values, and the nearest neighbor model (p = 0) produces poor synchronization. (D) Final SI values computed at the end of 8 cycle simulations and R values computed over the last 8 cycles of these simulations as a function of the probability p. For each p value, mean SI and R values (circles) and their standard deviations (error bars) were computed from the 10 network realizations. The large mean values and small standard deviations obtained for the small-world network model (p = 0.05, dashed line) show that additional shortcut connections (p > 0.05) do not enhance synchronization. (E) Final SI values obtained for small-world network models (p = 0.05) with different numbers of cells placed on the grid. For each cell number N, the mean SI value (circle) and its standard deviations (error bars) were computed from the 10 network realizations. The largest mean values and smallest standard deviations were obtained for $N \geq 225$, demonstrating that the combination of large cell numbers and long-range connections enhances synchronization of heterogeneous cell populations.**

behavior of different network architectures under environmental conditions of constant darkness. *Per* mRNA time profiles of 10 randomly selected cells from the population showed that limited long-range connectivity across the small-world network model (p = 0.05) eliminated arrhythmic cells and produced a highly phase synchronized population (Fig. 2A; VIP introduced at t = 150 h). VIP signaling caused individual *Per* mRNA profiles to display a rapid increase in amplitude similar to experimental data (Yamaguchi et al., 2003). Moreover, the predicted SI value of 0.93 obtained at the end of the simulation was close to the SI value of 0.90 calculated from SCN slice data (data not shown). By contrast, the nearest neighbor model (p = 0) with no long-range connections produced a fraction of arrhythmic cells and a poorly phase synchronized population after VIP introduction (Fig. 2B). Our results for locally connected networks differ from those of Kunz and Achermann (2003) because 1) our network is considerably more heterogeneous due to inclusion of ~80% non-VIPergic neurons, and 2) our model includes equally weighted connections with just the 4 nearest neighbors whereas the Kunz and Achermann model includes unequal weightings with many more neurons.

Rapid and nearly complete synchronization was observed for p = 0.05 and p = 1 when the cell

populations were coupled after 1 oscillation cycle (Fig. 2C). The inability of these networks to produce complete synchronization (SI = 1) was attributable to cellular heterogeneity rather than insufficient coupling as $p = 1$ corresponds to a fully coupled mean-field model. Although the small-world networks obtained for $p = 0.01$ exhibited a rapid increase in SI following coupling, the extent of long-range coupling was not sufficient to achieve the same degree of synchronization as the mean-field model. Despite its extensive local coupling, the nearest neighbor model ($p = 0$) was not able to produce a well-synchronized population and exhibited greater variability in SI values with time. The probability p had similar effects on SI values computed at the end of 8 cycle simulations and R values computed over the last 8 cycles of these simulations, showing that the effective dynamic range of the small-world network was $0.001 < p < 0.05$ (Fig. 2D). Both synchronization measures were monotonically increasing functions of p that reached their asymptotic values near our nominal probability $p = 0.05$. Comparatively small standard derivations in the synchronization measures were obtained for $p \geq 0.05$, showing that the small-world networks were able to consistently synchronize the cell populations despite heterogeneities in the 10 network realizations. These results demonstrate that a minimum amount of long-range coupling is necessary and sufficient to synchronize the heterogeneous cell populations.

We varied the number of cells N in the population to investigate the effect on synchronization behavior. For small cell numbers, SI values computed at the end of 10 cycle simulations with $p = 0.05$ were strongly dependent on N (Fig. 2E). Using 10 network realizations for each N, the average SI values decreased sharply and the standard deviations in SI were comparatively large for cell numbers below 100. By contrast, the average SI values and their standard deviations obtained were largely independent of N for 225 or more cells included in the population. These results demonstrate that our simulation results have not been inadvertently biased through the use of an insufficiently large cell population. Therefore, our model predictions suggest that large cell populations combined with long-range connectivity enhance the ability of heterogeneous circadian oscillators to phase synchronize.

We varied the probability p to investigate the relationship between network architecture and the resulting fractions of rhythmic cells and their period distributions. As discussed earlier, random perturbations in the

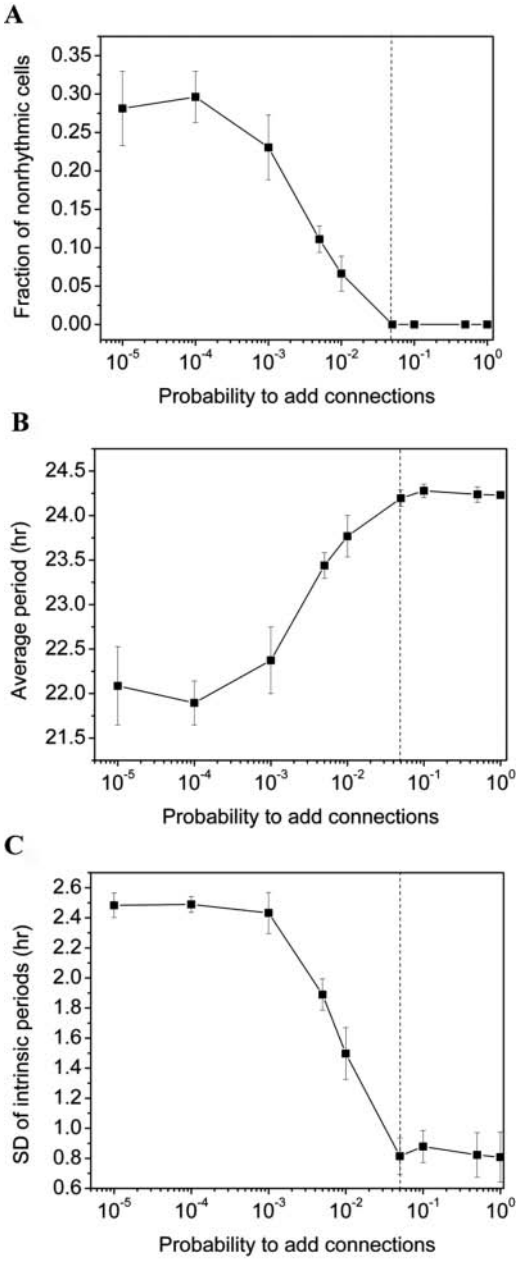

Figure 3. The relationship between the network architecture and the resulting fractions of rhythmic cells and their period distributions. For each probability value, the mean (circle) and standard deviation (error bars) were computed from 10 network realizations. (A) The fraction of nonrhythmic cells as a function of the probability p. The population consisted of approximately 30% nonrhythmic cells for small p values, whereas the nonrhythmic population was completely eliminated in the small-world region ($p = 0.05$) where synchronization was enhanced. (B) The mean period reached a near maximal value of 24.2 h for $p = 0.05$ (dashed line) and decreased uniformly to 22.0 h for $p = 0$, suggesting that long-range connectivity improves the accuracy of circadian timekeeping. (C) The standard deviation of the period distribution reached a maximum of 2.5 h at $p = 0$ and decreased uniformly until a near minimal value of 0.8 h was reached at $p = 0.05$ (dashed line), suggesting that long-range connectivity enhances the precision of circadian timekeeping.

basal *Per* transcription rate (ν_{sp0}) were introduced to create an uncoupled population in which about 40% of the model neurons were intrinsically rhythmic. From 10 network realizations, the nearest neighbor model ($p = 0$) produced an average of approximately 70% rhythmic cells and 30% nonrhythmic cells (Fig. 3A) due to the local coupling that remains in the absence of long-range connections. The percentage of nonrhythmic cells decreased to 0% at $p = 0.05$ as a result of increased long-range coupling.

As p was increased, the mean period of the population increased with an asymptotic value of approximately 24.2 h reached for $p = 0.05$ (Fig. 3B). By contrast, the nearest neighbor model ($p = 0$) produced a smaller mean period of approximately 22.0 h. Using 10 network realizations for each p value, comparatively small standard deviations in the mean periods were obtained for $p \geq 0.05$. We also computed standard deviations of the individual neuron periods for each network realization. When these standard deviations were averaged across 10 realizations for each p value, networks with small p values (few long-range connections) produced much larger period variability than larger p values (Fig. 3C). These mean values reached an asymptotic small value of approximately 0.8 h at $p = 0.05$, with additional coupling unable to further reduce the period variability. Our computational results suggest that the limited long-range connections in the small-world network models enhanced the accuracy of circadian timekeeping with respect to a 24-h cycle and enhanced precision by decreasing the period variability across the population.

Intracellular Signaling in Small-World Networks

We varied the probability p to investigate the effect on the signal transduction mechanism under constant darkness. We evaluated the circadian coordination of each network via the amplitudes of 2 key signaling components, VIP and cAMP response element binding protein (CREB). VIP was used as an indicator of circadian output and of cell-to-cell signaling (Aton et al., 2005), and CREB was used as an indicator of the drive on the circadian pacemaker (Nielsen et al., 2002). For each network realization, we averaged the VIP and CREB amplitudes of individual cells across the population of 400 neurons at each time point to calculate the average amplitude of these 2 physiological indicators. These values were used to compute the average and standard deviation across 10 different network realizations for each p value,

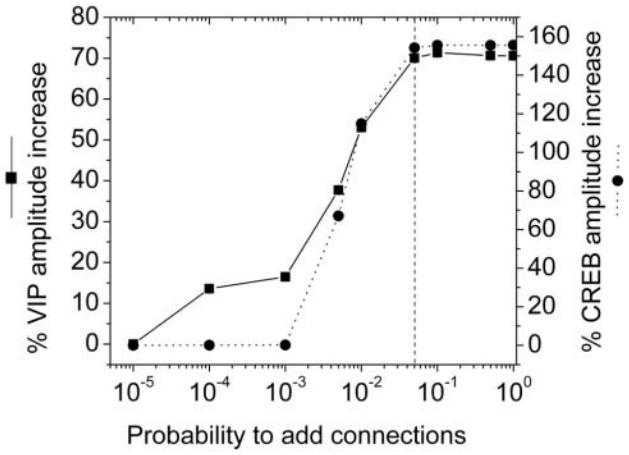

Figure 4. Percent increases in vasoactive intestinal polypeptide (VIP) and cAMP response element binding protein (CREB) oscillation amplitudes as a function of the probability *p*. The VIP (solid line) and CREB (dotted line) amplitudes obtained for the nearest neighbor model ($p = 0$) were used to scale the results. For each probability value, the mean (circle) and standard deviation (error bars) were computed from 10 network realizations. The mean amplitudes reached a maximum in the small-world region ($p = 0.05$, dashed line) and decreased uniformly with decreasing *p*.

with the results plotted in terms of amplitude increases from the nearest neighbor model ($p = 0$). Low probability values resulted in relatively low amplitude average VIP and CREB oscillations (Fig. 4), because of substantial populations of nonrhythmic cells (Fig. 3A) and a lack of synchronized rhythms among rhythmic cells (Fig. 2D) at these p values. Circadian rhythms dramatically increased in amplitude above $p = 10^{-3}$, with maximal values nearly achieved with our nominal probability $p = 0.05$ corresponding to the small-world network topology. These results provide further evidence that long-range connections in the small-world network model coordinate individual cell dynamics and mediate population synchronization.

Light Entrainment in Small-World Networks

We varied the probability p for different light schedules to determine their combined effects on synchronization behavior. Three schedules were considered: constant darkness (DD), constant light (LL), and 12 h of constant light followed by 12 h of constant darkness (LD). Photic input was assumed to enhance *Per* transcription through the same signaling cascade as VIP (To et al., 2007). For each p value, 10 network realizations were generated and simulated for the calculation of the average SI and its standard deviation. The DD results

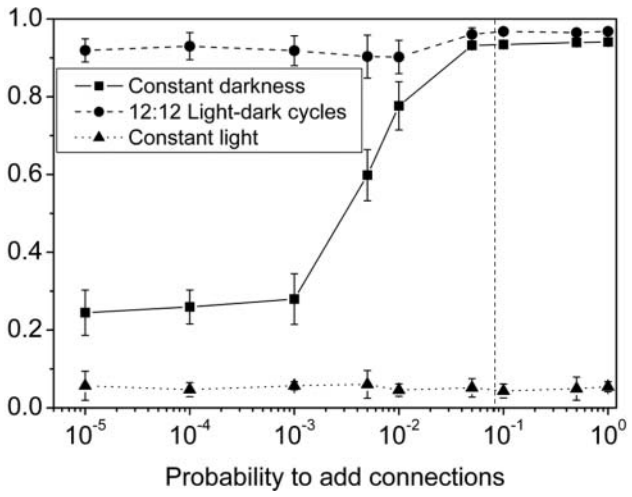

Figure 5. The effect of different light schedules and the probability p on the synchronization index SI. For each light schedule and p value, the mean (circle) and standard deviation (error bars) were computed from 10 network realizations. A large increase in the mean SI value for constant darkness (solid line) was observed in the small-world region with a near maximal value obtained for p = 0.05 (dashed line). Constant light (dotted line) produced poor synchronization for all p values despite complete elimination of the nonrhythmic cell population present for constant darkness with $p < 0.05$, demonstrating a lack of synchronization among oscillating cells rather than a lack of rhythmicity at the single cell level. Schedules with alternating 12 h of light and darkness (dashed line) produced strong synchronization for all p values, suggesting that long-range connectivity may not be essential when light entrains the cell population.

repeated from Figure 2D show that a highly synchronized population was only achieved for p values in and above the small-world region including our nominal value $p = 0.05$ (Fig. 5). The LD cycles produced larger SI values regardless of the p value used, suggesting that the presence of long-range connections is less critical for synchronization when individual cells are exposed to alternating light-dark cycles. By contrast, LL failed to produce a synchronized population regardless of the p value used. Such behavior is supported by experiments in which exposure to constant bright light abolished circadian synchrony across the population (Ohta et al., 2006). Our computational results suggest that the primary advantage of small-world networks is to promote synchronization among sparsely connected populations in the absence of light.

In addition to affecting the degree of synchrony across the population, exposure to different light schedules was found to influence the rhythmic phenotype of individual neurons. Introduction of light to sparsely connected networks ($p < 0.05$) increased the propensity of neurons to oscillate as the approximately 30% of nonrhythmic cells in DD (Fig. 3A) were completely eliminated during LL and LD cycles (data not shown). The absence of nonrhythmic cells under LL conditions shows that the low SI values obtained for constant light are attributable to a lack of synchronization among oscillating cells rather than a lack of rhythmicity at the single-cell level. The small-world network model with $p = 0.05$ produced 100% oscillating cells and individual *Per* mRNA profiles of similar amplitude regardless of the light schedule implemented, suggesting that a minimal level of long-range connectivity is sufficient to eliminate nonrhythmic cells. Taken together, these results suggest a possible correlation between light exposure and rhythmicity, with limited intercellular connectivity allowing photic signals to drive additional SCN neurons to sustained oscillations.

DISCUSSION

Small-World Network Models for Circadian Organization

The SCN consists of a heterogeneous population of neurons that can be placed in distinct functional groups depending on their rhythmic behavior, their neuropeptide content, and their ability to perceive light (Antle and Silver, 2005). The objective of this study was to investigate the relationship between the neural network architecture and the resulting behavioral phenotypes. We combined a detailed molecular description of the core mammalian circadian oscillator (Leloup and Goldbeter, 2003) with a simplified description of the VIP signaling cascade (To et al., 2007) to generate a single cell model capable for intercellular communication. Random perturbations were introduced in selected core oscillator model parameters such that the resulting cell population was heterogeneous with respect to uncoupled rhythmic behavior. A 2-dimensional grid was populated with 400 heterogeneous model cells that were coupled using different schemes that ranged from the nearest neighbor model to the mean-field model. Intermediate coupling patterns were generated through the addition of shortcut connections between random pairs of cells according to a probability p. Probability values in range $0.01 < p < 0.1$ yielded small-world network models characterized by local circuits of tightly coupled cells combined with random long-range connections (Newman et al., 2000; Watts and Strogatz, 1998). Heterogeneity in VIP synthesis was captured by randomly zeroing VIP production from 80% of the model

neurons and eliminating all connections from these non-VIPergic cells, resulting in networks with nonreciprocal as well as reciprocal connections.

We varied the probability p of adding shortcut connections and investigated the effect on the structural and dynamical properties of the resulting neural networks. Our main finding was that a small-world network model ($p = 0.05$) was able to produce similar SI values as the mean-field model despite having only 10% of the total possible connections. Because signal transmission via action potentials requires high energy expenditure, connecting distant neurons across the brain is a costly mechanism (Attwell and Laughlin, 2001). From this perspective, small-world networks can be interpreted as generating more efficient connectivity patterns than the mean-field model while producing the same functional performance with regard to cellular synchronization and rhythm generation. The nearest neighbor model was not able to produce a well-synchronized population, suggesting the importance of long-range connections in coordinating the activity of heterogeneous SCN neurons. By varying the number of cells in the population, we found that larger cell populations combined with long-range connectivity enhanced the ability of the heterogeneous circadian oscillators to phase synchronize. The role of long-range connections to synchronize distant circadian oscillators may be relevant to the observation that separating the dorsal and ventral SCN abolishes synchrony in the dorsal SCN (Yamaguchi et al., 2003), perhaps by selectively cutting long-range VIP connections from the ventral SCN.

We found that the probability p had a strong effect on the fraction of rhythmic cells, with approximately 30% of cells nonrhythmic for small p values and the population of non-rhythmic cells disappearing entirely in the small-world region ($p = 0.05$). As p was increased, the mean period of the rhythmic cells increased (22.0 to 24.2 h) and the standard deviation of the mean periods computed from 10 network realizations for each p value decreased (2.5 to 0.8 h). These model predictions are consistent with data collected from cultures lacking VIP intercellular signaling that exhibited a reduced proportion of neurons that fired rhythmically, a decreased average period of approximately 22 h, and broadened distributions of individual periods (Aton et al., 2005; Brown et al., 2005). However, our model predicted that the introduction of a non-VPAC2-expressing population would inhibit synchronization, suggesting that the model may require additional intercellular coupling mechanisms to reproduce experimental observations (King et al., 2003).

Model Implications for Age-Related Circadian Dysfunction

Senescence has been associated with decreased VIP and CREB amplitudes (Kallo et al., 2004), reduced mean periods (Aujard et al., 2006; Pittendr and Daan, 1974), and lower percentages of neurons able to fire rhythmically (Nygard et al., 2005). Our small-world network model provides a potential mechanism to explain decreased synchronicity and reduced circadian function in the aged SCN. We showed that decreasing the probability p to add shortcut connections produced reduced VIP and CREB amplitudes (Fig. 4), shorter mean periods (Fig. 3B), and a larger percentage of nonrhythmic cells (Fig. 3A) compared with a more highly connected network. These results suggest a possible connection between the loss of long-range connections between otherwise fully functional neurons and age-related circadian dysfunction.

However, available data concerning the precision of the individual neurons with aging are contradictory and have shown both preservation of the clock gene profiles (Asai et al., 2001) and lower amplitude oscillations (Weinert et al., 2001). Similarly, the effect of senescence on the number of SCN neurons has not been resolved, with some studies showing that aging does not affect the quantity of cells within the SCN (Madeira et al., 1995) whereas other studies have shown that senescence is accompanied by the depletion of SCN neurons (Tsukahara et al., 2005). Our results (Fig. 3E) suggest that an extensive loss of SCN neurons may also lead to a decrease in synchrony indicative of senescence. Taking these data into consideration, our model predicts that partial loss of long-range VIP connections between otherwise fully functional neurons may contribute to age-related deterioration of circadian function.

ACKNOWLEDGMENTS

This work was supported by the National Institutes of Health grant GM078993 and the National Science Foundation–sponsored Institute for Cellular Engineering IGERT program DGE-0654128.

REFERENCES

Abrahamson EE and Moore RY (2001) Suprachiasmatic nucleus in the mouse: Retinal innervation, intrinsic organization and efferent projections. Brain Res 916:172-191.

Albert R and Barabasi AL (2002) Statistical mechanics of complex networks. Rev Mod Phys 74:47-97.

Antle MC, Foley DK, Foley NC, and Silver R (2003) Gates and oscillators: A network model of the brain clock. J Biol Rhythms 18:339-350.

Antle MC and Silver R (2005) Orchestrating time: Arrangements of the brain circadian clock. Trends Neurosci 28:145-151.

Asai M, Yoshinobu Y, Kaneko S, Mori A, Nikaido T, Moriya T, Akiyama M, and Shibata S (2001) Circadian profile of Per gene mRNA expression in the suprachiasmatic nucleus, paraventricular nucleus, and pineal body of aged rats. J Neurosci Res 66:1133-1139.

Aton SJ, Colwell CS, Harmar AJ, Waschek J, and Herzog ED (2005) Vasoactive intestinal polypeptide mediates circadian rhythmicity and synchrony in mammalian clock neurons. Nat Neurosci 8:476-483.

Attwell D and Laughlin SB (2001) An energy budget for signaling in the grey matter of the brain. J Cerebral Blood Flow Metab 21:1133-1145.

Aujard F, Cayetanot F, Bentivoglio M, and Perret M (2006) Age-related effects on the biological clock and its behavioral output in a primate. Chronobiol Int 23:451-460.

Bernard S, Gonze D, Cajavec B, Herzel H, and Kramer A (2007) Synchronization-induced rhythmicity of circadian oscillators in the suprachiasmatic nucleus. Plos Comput Biol 3:667-679.

Brown TM, Hughes AT, and Piggins HD (2005) Gastrin-releasing peptide promotes suprachiasmatic nuclei cellular rhythmicity in the absence of vasoactive intestinal polypeptide-VPAC(2) receptor signaling. J Neurosci 25:11155-11164.

Cherniak C (1992) Local optimization of neuron arbors. Biol Cybern 66:503-510.

Daikoku S, Hisano S, and Kagotani Y (1992) Neuronal associations in the rat suprachiasmatic nucleus demonstrated by immunoelectron microscopy. J Comp Neurol 325:559-571.

Dardente H, Menet JS, Challet E, Tournier BB, Pevet P, and Masson-Pevet M (2004) Daily and circadian expression of neuropeptides in the suprachiasmatic nuclei of nocturnal and diurnal rodents. Mol Brain Res 124:143-151.

Garcia-Ojalvo J, Elowitz MB, and Strogatz SH (2004) Modeling a synthetic multicellular clock: Repressilators coupled by quorum sensing. Proc Natl Acad Sci U S A 101:10955-10960.

Gonze D, Bernard S, Waltermann C, Kramer A, and Herzel H (2005) Spontaneous synchronization of coupled circadian oscillators. Biophys J 89:120-129.

Henson MA (2004) Modeling the synchronization of yeast respiratory oscillations. J Theor Biol 231:443-458.

Kalamatianos T, Kallo I, Piggins HD, and Coen CW (2004) Expression of VIP and/or PACAP receptor mRNA in peptide synthesizing cells within the suprachiasmatic nucleus of the rat and in its efferent target sites. J Comp Neurol 475:19-35.

Kallo I, Kalamatianos T, Piggins HD, and Coen CW (2004) Ageing and the diurnal expression of mRNAs for vasoactive intestinal peptide and for the VPAC(2) and PAC(1) receptors in the suprachiasmatic nucleus of male rats. J Neuroendocrinol 16:758-766.

King VM, Chahad-Ehlers S, Shen S, Harmar AJ, Maywood ES, and Hastings MH (2003) A hVIPR transgene as a novel tool for the analysis of circadian function in the mouse suprachiasmatic nucleus. Eur J Neurosci 17: 822-832.

Kunz H and Achermann P (2003) Simulation of circadian rhythm generation in the suprachiasmatic nucleus with locally coupled self-sustained oscillators. J Theor Biol 224:63-78.

Leloup JC and Goldbeter A (2003) Toward a detailed computational model for the mammalian circadian clock. Proc Natl Acad Sci U S A 100:7051-7056.

Low-Zeddies SS and Takahashi JS (2001) Chimera analysis of the Clock mutation in mice shows that complex cellular integration determines circadian behavior. Cell 105:25-42.

Madeira MD, Sousa N, Santer RM, Paulabarbosa MM, and Gundersen HJG (1995) Age and sex do not affect the volume, cell numbers, or cell-size of the suprachiasmatic nucleus of the rat—An unbiased stereological study. J Comp Neurol 361:585-601.

Mitchison G (1991) Neuronal branching patterns and the economy of cortical wiring. Proc R Soc Lond Biol 245:151-158.

Moore RY, Speh JC, and Leak RK (2002) Suprachiasmatic nucleus organization. Cell Tissue Res 309:89-98.

Netoff TI, Clewley R, Arno S, Keck T, and White JA (2004) Epilepsy in small-world networks. J Neurosci 24:8075-8083.

Newman MEJ (2000) Models of the small world. J Stat Phys 101:819-841.

Newman MEJ, Moore C, and Watts DJ (2000) Mean-field solution of the small-world network model. Phys Rev Lett 84:3201-3204.

Nielsen HS, Hannibal J, and Fahrenkrug J (2002) Vasoactive intestinal polypeptide induces per1 and per2 gene expression in the rat suprachiasmatic nucleus late at night. Eur J Neurosci 15:570-574.

Nygard M, Hill RH, Wikstrom MA, and Kristensson K (2005) Age-related changes in electrophysiological properties of the mouse suprachiasmatic nucleus in vitro. Brain Res Bull 65:149-154.

Ohta H, Mitchell AC, and McMahon DG (2006) Constant light disrupts the developing mouse biological clock. Pediatr Res 60:304-308.

Pennartz CMA, De Jeu MTG, Geurtsen AMS, Sluiter AA, and Hermes M (1998) Electrophysiological and morphological heterogeneity of neurons in slices of rat suprachiasmatic nucleus. J Physiol (Lond) 506:775-793.

Pittendr CS and Daan S (1974) Circadian oscillations in rodents—Systematic increase of their frequency with age. Science 186:548-550.

Reppert SM and Weaver DR (2002) Coordination of circadian timing in mammals. Nature 418:935-941.

Romijn HJ, Sluiter AA, Pool CW, Wortel J, Buijs RM, et al. (1997) Evidence from confocal fluorescence microscopy for a dense, reciprocal innervation between AVP-, somatostatin-, VIP/PHI-, GRP- and VIP/PHI/GRP-immunoreactive neurons in the rat suprachiasmatic nucleus. European Journal of Neuroscience 9:2613-2623.

Sporns O, Chialvo DR, Kaiser M, and Hilgetag CC (2004) Organization, development and function of complex brain networks. Trends Cogn Sci 8:418-425.

Strogatz SH (2000) From Kuramoto to Crawford: Exploring the onset of synchronization in populations of coupled oscillators. Physica D 143:1-20.

Strogatz SH (2001) Exploring complex networks. Nature 410:268-276.

To TL, Henson MA, Herzog ED, and Doyle FJ (2007) A molecular model for intercellular synchronization in the mammalian circadian clock. Biophys J 92:3792-3803.

Tsukahara S, Tanaka S, Ishida K, Hoshi N, and Kitagawa H (2005) Age-related change and its sex differences in histoarchitecture of the hypothalamic suprachiasmatic nucleus of F344/N rats. Exp Geront 40:147-155.

Watts DJ, Strogatz SH (1998) Collective dynamics of 'small-world' networks. Nature 393:440-442.

Weinert H, Weinert D, Schurov I, Maywood ES, and Hastings MH (2001) Impaired expression of the mPer2 circadian clock gene in the suprachiasmatic nuclei of aging mice. Chronobiol Int 18:559-565.

Yamaguchi S, Isejima H, Matsuo T, Okura R, Yagita K, Kobayashi M, and Okamura H (2003) Synchronization of cellular clocks in the suprachiasmatic nucleus. Science 302:1408-1412.